A facile method to fabricate the durable and self-protective coating for marine applications

Hao Yang [a], Liguo Qin [a,*], Fei Wang [b], Fagla Jules Mawignon [a], Mochen Dong [c], Yuhao Wu [a], Yali Zhang [b], Zeyu Ma [a]

[a] *Key Laboratory of Education Ministry for Modern Design and Rotor-Bearing System, Institute of Design Science and Basic Components, School of Mechanical Engineering, Xi'an Jiaotong University, 710049, PR China*
[b] *Key Laboratory of Biomedical Information of Ministry of Education, School of Life Science and Technology, Xi'an Jiaotong University, 710049, PR China*
[c] *School of Chemistry, Cardiff University, Cardiff CF10 3AT, United Kingdom*

ARTICLEINFO

Keywords:
Slippery liquid infused surface
Anti-fouling
Anti-corrosion
Durability

ABSTRACT

Endowing coatings with effective protective function for metal substrates is of great interest. An excellent example is slippery liquid infused surface (SLIS) which possesses potential applications owing to its unique liquid repellency and self-cleaning properties. However, their widespread applications are facing obstacles of complex preparation, poor protection and low durability. Herein, a facile and efficient liquid infusion method was proposed to construct SLIS by altering the heterogeneous microstructure on the SiO_x layer of the coatings with direct UV irradiation. The coatings were fabricated by conducting an appropriate UV irradiation treatment on polydimethylsiloxane (PDMS) film infused with methyl oleate (MO). The as-prepared transparent anti-fouling coatings showed outstanding anti-fouling properties against various contaminants such as algal (Chlorella), sand, rust (Fe_2O_3), paints (both water-based and oil-based) and daily life liquid pollutants (e.g., water, coffee, cola, soy sauce and milk). In addition, results revealed that the coatings exhibited a prominent anti-corrosion performance. Moreover, the coatings had excellent mechanical, chemical and thermal durability regarding the great repellency of the pollutants. We proposed this synergistic strategy between lubricant infusion and coating heterogeneous microstructure to widen new possibilities for fabricating coatings with promissing anti-corrosive and anti-fouling functionality.

1. Introduction

The past decades have witnessed considerable efforts in solving the global marine fouling challenge faced by the whole marine industry. The focus should be emphasized on the development of protective coatings for wading surfaces to avoid or mitigate the great economic losses and serious environmental pollution problems incurred by fouling and corrosion [1–3]. Anti-fouling coatings stand for the films fabricated on surfaces that can prevent contamination [4]. From the point of surface wettability, anti-fouling coatings generally refer to the solid surfaces driving out liquids [5]. When the surfaces are titled, the liquids can slide away and bring off the pollutants simultaneously, granting the anti-fouling property to the solid surfaces. From the perspective of anti-corrosion, corrosion resistance performance is necessary to be also considered during the fabrication of anti-fouling surfaces. In fact, when the metal substrate corrodes, the complex chemical environment existing on the surface may destroy the morphology and provide strong adhesion conditions for various organic and inorganic contaminants [6]. Therefore, anti-fouling performance of coatings is also a very important index for estimating the service property [7].

The anti-fouling performance is closely related to surface wettability and chemical composition. In the field of surface wettability, some specific superhydrophobic surfaces with micro-nano structures [8], such as lotus leaf and rice leaf, have received continuous attention due to their excellent liquid repellency, where the liquid droplets have super high contact angles (CA) and could easily roll off with small sliding angles (SA). However, there are some drawbacks in the super-hydrophobic surfaces technology [9] as following: Firstly, traditional fabrication methods for micro-/nanostructures are generally etching [10], electrochemistry [11] and electrospinning [12], etc., which not only have complicated processes but also show low production effi- ciency. Of course, there are also several facile methods developed to

* Corresponding author.
E-mail address: liguoqin@xjtu.edu.cn (L. Qin).

produce superhydrophobic surfaces such as the deposition of nanoparticles. However, when exposed to prolonged UV-radiation, these self-cleaning materials raise lots of concerns about the stability of the hydrophobic properties [13]. Secondly, the gas film, relying on the Cassie effect and adhering to micro-nano structures, is not stable [14]. Once faced the high pressure, high humidity and long-term service conditions, the gas film could be easily broken down, leading to the loss of its repelling ability [15] and the pollution of the surface [16]. Thirdly, poor optical transparency is also a weakness of superhydrophobic coatings [17].

Another strategy to achieve an anti-fouling surface is to construct slippery surfaces, which are not superhydrophobic, but liquid droplets that can roll off because of the quite low SA [18]. In recent years, varieties of novel slippery anti-fouling surfaces have been proposed. For instance, slippery liquid-infused surfaces (SLIS) [19], liquid-like monolayer membranes [20] and polymer brush molecular layers [21]. Despite the low CA, these smooth anti-fouling surfaces have many advantages compared to the micro-/nanostructured anti-fouling surfaces such as transparency and stability. Among them, the SLIS has gained more attention due to its facile preparation, high stability and environmental friendliness.

In 2011, Wong's group [22] firstly proposed the concept of a liquid infused porous surface (lubricant infused Surface, LIS) or a slippery liquid infused porous surface (Slippery liquid infused surfaces, SLIS). SLIS employed both the capillary force and van der Waals force to lock non-toxic and chemical inert oils in the stable surface [23]. Compared to the superhydrophobic surface, a more stable "solid/liquid composite film layer" was formed due to the porous structure of SLIS when they were immersed into liquids with low surface energy. By now, various methods, such as spraying coatings [24], chemical and physical etching [25], sol-gel synthesis [26], and so on have been used to fabricate SLIS. Fluor alkyl layers are generally grafted on porous substrates to reduce the surface free energy to form stable SLIS [27]. At the same time, PFPE (such as DuPont Krytox oil) is used as a lubricant owing to its good compatibility with fluorinated surfaces [28]. However, due to economic and ecological damages caused by fluorinated compounds, cost-effective and eco-friendly alternatives should be promoted in marine applications for SLIS [29]. Aizenberg et al. [30] prepared the nanostructured surfaces by deposition of negatively charged silica nanoparticles layer and positively charged polyelectrolyte layer, and then filled fluorinated oils into the surfaces to develop SLIS. This method has strict requirements for devices' preparation. SLIS was also prepared by infusing various silicone oils in sol–gel derived nanocomposite coatings [26], which had excellent liquid repelling properties but the anti-fouling performance was weakened and disappeared as the lubricant was consumed or replaced by pollutants. Moreover, using polymer brushes, Zheng et al. [31] fabricated SLIS which only stretched and contracted around their planted position and could not move in a wide translational range, leading to no super excellent anti-fouling performance. Concerning the anti-corrosion performance of SLIS, it was reported that benzotriazole (BTA) is appropriate to be used as corrosion inhibitor encapsulated in anti-corrosion coatings, whose derivatives are quite effective inhibitors for corrosion protection of steel [32]. However, whenever coatings were mixed directly with the corrosion inhibitors, the BTA molecules were easily dissolved into the aqueous solution, leading to the appearance of micro-pores in the coating and the failure of corrosion resistance [33]. Therefore, the construction of SLIS with stable anti-fouling and anti-corrosion is dedicated tremendous efforts.

Here, we fabricated a durable, self-cleaning, corrosion-resistant, environmentally friendly and transparent anti-fouling coating appli- cable onto the metal substrate. First, a transparent coating was prepared through the condensation reaction of PDMS with curing agent addition, and meanwhile UV irradiation was employed during the curing process for cross-linking. Then the lubricant MO was infused into the silicone coating for an anti-fouling function. The as-obtained transparent coatings investigated excellent anti-fouling properties against various fluids. Results showed notable repelling behaviors on water and other liquid pollutants in daily life (such as coffee, cola, soy sauce and milk), while for organic (such as Chlorella) and inorganic contaminants (such as sand particles and daily common rust particles), prominent resistance was observed. In addition, the corrosion behaviors of SLIS in seawater were observed with Tafel plots and electrochemical impedance spectroscopy (EIS) by electrochemical test. Fabricated SLIS displayed excellent protective effects on the metal substrate with strong anti-corrosion properties. Furthermore, the coatings showed outstanding and durable mechanical, chemical and thermal performance. It is distinguished that these SLIS coatings are different from the existing anti-fouling coatings because of the facile preparation method, and also, their excellent anti-fouling, anti-corrosion and stable properties will be introduced at length in the following parts, providing distinct inspirations for developing effective anti-fouling and anti-corrosion coatings.

2. Experimental procedure

2.1. Materials

PDMS precursor was purchased from Dow Corning Co., Ltd., America. MO was obtained from TCI Co., Ltd., Japan. Sodium chloride (NaCl) and deionized water were purchased from China National Medicines Co. Ltd. All chemical reagents are of analytical grade and were used without further purification. The soil was collected in the garden and the rust was prepared by the oxidation of pure iron in the air. The daily liquid pollutants, water-based stamp and oil-based stamp were purchased online.

2.2. Preparation of durable anti-fouling surfaces

The PDMS base and curing agent were mixed at a ratio of 10:1, then poured into beaker, placed on the magnetic stirrer (Yuezhong Instrument Equipment Co., Ltd. Shanghai) and stirred for 3 min to be totally mixed. Then, the mixture was applied onto the clean Q235 steel substrate to obtain four sets of samples. In order to improve the cross-linking of PDMS for enhancing the locking performance of MO, UV-treatment was used before the two PDMS precursors were fully cured. The UV irradiation time was set to 0, 45, 90 and 135 min, respectively. The lubricant MO with a concentration of 20 μL/cm^2 was used to prepare SLIS. The lubricant was automatically trapped inside the samples through capillary effect. After immersing in MO solution for 24 h, four different groups of specimens were prepared according to the UV irradiation time (MOPDMS, 45UV-MOPDMS, 90UV-MOPDMS 135UV-MOPDMS). Each group contained more than 15 identical and independent samples, so that each subsequent characterization experiment can be repeated at least three times to approve the reproducibility of the data. After the infusion, samples were stored at 60 °C for 24 h. Any excess lubricant was removed gravimetrically by tilting the surfaces at an angle of approximately 90°. Finally, samples were stored at room temperature for 24 h for further study. Except for electrochemical test, experiments were conducted on the SLIS coatings without metal substrate.

2.3. Characterization

The static CA and SA of various liquids (5 μL) on the surface of the samples were measured using a Contact Angle System JC2000D2A, (China) equipped with a tilting platform. Through the sessile drop method, the reported data were the calculated average value of five readings at different places on samples. The surface morphology of samples was captured by a field emission scanning electron microscope (MAIA3 LMH, USA). FTIR spectra results were recorded from Fourier Transform Infrared Spectroscopy (Nicolet iS50, China) equipped with an MVP-PRO Attenuated Total Reflection (ATR) unit (diamond crystal, 45° angle of incidence) and a KBr beam splitter. A scanning range of

550–4000 cm^{-1} with a resolution of 4 cm^{-1} and average over 100 scans were used. The baseline correction of FTIR spectra was performed using concave rubber band correction method with the OPUS software (Version 8.5, Bruker optics incorporation).

It is well-known that the most important step for forming marine fouling organisms is the formation of biofilm, which can provide nutrients for the offspring of large fouling organisms as well as greater adhesion for all kinds of micro-organisms. Therefore, Chlorella, a unicellular algae distributed worldwide, was selected to test the anti-adhesion ability. After mixing pure water, chlorella seeds and culture medium in a mass ratio of 50:2:1, the mixture was poured into a transparent glass beaker. When room temperature was around 25 °C, the mixed liquid was kept in the natural light environment and stirred every 4 h every day. After 5 days, the color gradually changed to green, then it could be used as an anti-fouling test solution rich in Chlorella. After immersing the coatings in Chlorella solution for three days, surfaces were washed with water and the morphological observation and measurement of Chlorella were performed using an inverted optical microscope (CKX53, Olympus, Japan) equipped with a digital camera and computer.

2.4. Mechanical and chemical stability tests

To observe lubricant stable releasing in SLIS, the sample was placed on a shaking bed (ZLWY-100B, Shanghai) with the stroke of 20 mm under constant shaking of 80 rpm. Fresh deionized water was replaced every 12 h and the whole released procedure was kept for seven days. The fluorescence confocal microscopy (Leica TCS SP8 STED 3×, Germany) was used to directly visualize the MO infusion amount in the PDMS. And the captured confocal images were analyzed in semi-quantitative method to observe the fluorescence intensity with the software Image J. For mechanical stability, the samples were cut into rectangles with a length of 30 mm and a width of 10 mm, and were then subjected to cyclic stretching using the American INSTRON 5965 double-column desktop universal material testing machine. The load accuracy and the upper strain limit were set to 0.5 % and 100%, respectively. Chemical stability tests were carried out by soaking the coatings in various corrosive liquids, including 3.5 % $NaCl_{(aq)}$ and hot (60) water for a period of time. And after all the stability tests, the anti-fouling performance was recorded to evaluate stability of the coatings.

3. Results and discussion

3.1. Preparation of durable anti-fouling surfaces

As shown in Fig. 1(a), for the preparation of the SLIS, MO was absorbed by ultraviolet ray (UV) irritated-PDMS coatings. After stripping the coating from the Q235 substrate, the SLIS coating surfaces were quite smooth without any defects and the words "XJTU" could be clearly observed (Fig. 1b), indicating the substrate of high transparency and quality coatings. And the morphology of SLIS was also observed with Scanning Electron Microscope (SEM) in Fig. 1c. The SLIS could be readily prepared by irritating the PDMS substrates with UV-ray to plenty suck the lubricant MO.

3.2. FTIR spectra

The cross-linking of PDMS exposed to UV radiation in air atmosphere has been proposed in Fig. 2 [34]:

After the lubricant MO was infused, the chemical compositions of samples were further studied by ATR-FTIR measurement (Fig. 3). For pure PDMS, the peaks at 789–796 cm^{-1} were attributed to the $–CH_3$ rocking and Si—C stretching vibrations in Si–CH3 bonds; the peaks at 1074 cm^{-1}, 1260 cm-1 and 2965 cm^{-1} were owing to Si–O–Si stretching; and both $–CH^3$ deformation and asymmetric $–CH_3$ stretching were for $Si–CH_3$. The characteristic peaks of MO at 1409 cm^{-1}, 2852 and 2922 cm^{-1} were attributed to the $-CH_3$ umbrella mode, asymmetric and symmetric CH_2 stretches, respectively. The most intense characteristic peak at 1710 cm^{-1} was attributed to the stretching mode of –C=O. Furthermore, the presence of an ester group in MO was revealed by a broad characteristic band at 3300 cm^{-1} and the –C–O–C– moiety was detected by the band at 1172 cm^{-1}. To increase the hydrophilic performance of PDMS surfaces, oxidizing the polymer surface with plasma or UV irradiation is the established way. These processes are reported to be the facile way for the formation of a smooth oxidized surface layer of SiO_x [35]. The existence of SiO_x layer was identified by FTIR spectra (Fig. 3).

For the SLIS, characteristic peaks of MO were observed and MO

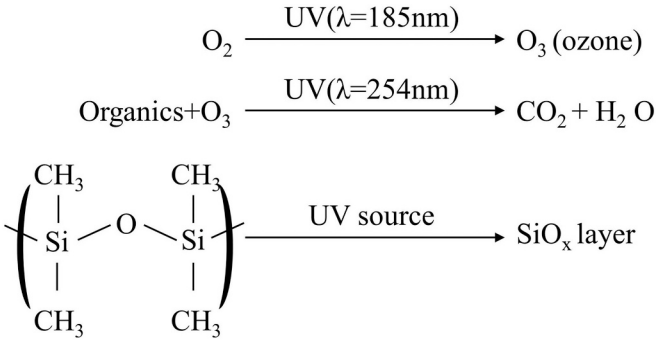

Fig. 2. The chemical schematic of PDMS cross-linking induced by UV-ray.

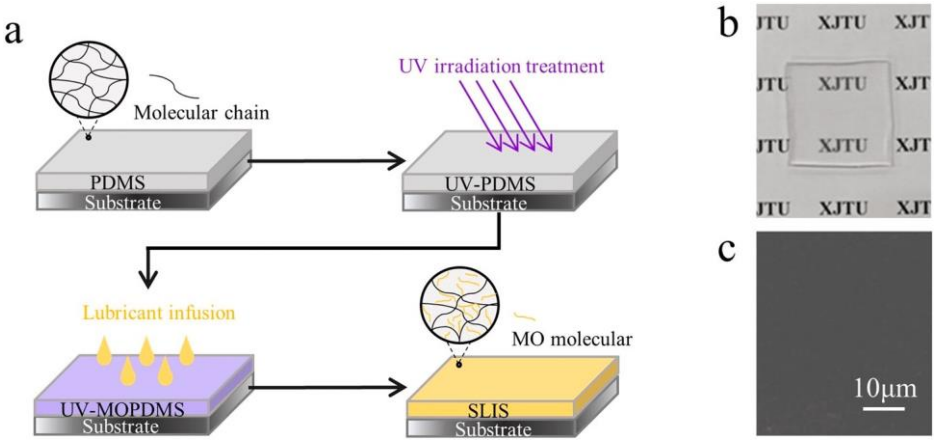

Fig. 1. The preparation process and transparent coatings.

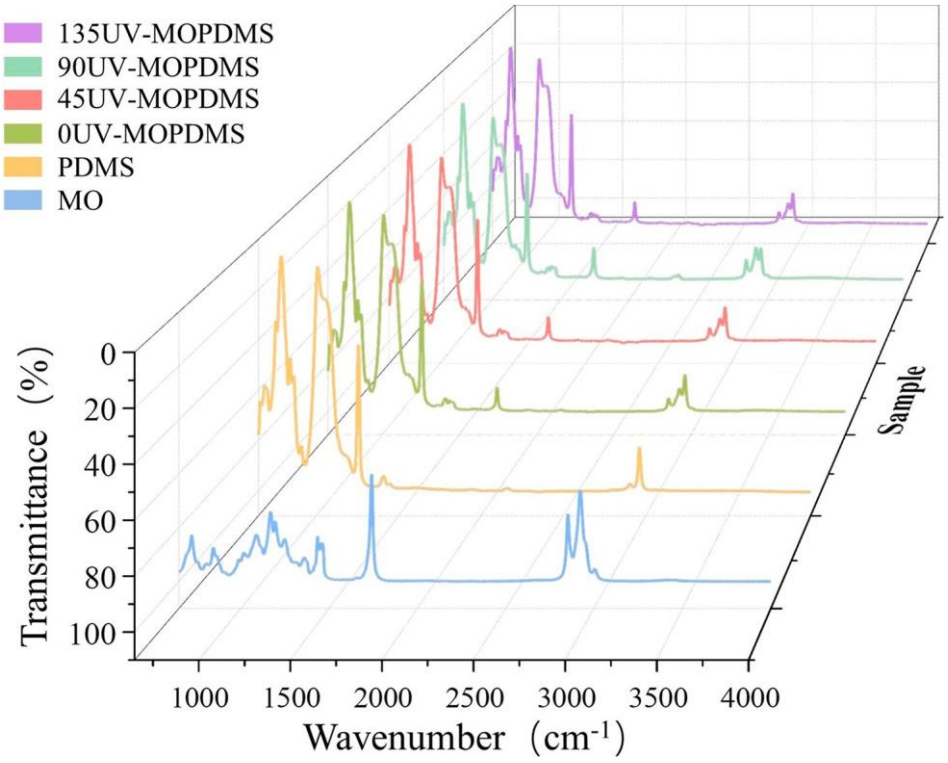

Fig. 3. (a) FTIR spectra of samples.

content was calculated with the P. Kowalik method [36]. For example, the characteristic peak at 2852 cm^{-1} attributed to the -CH_3 umbrella mode showed a trend of first increase and then decreasing in intensity while the UV irradiation time increased. The ratio of corresponding peak intensities of MOPDMS, 45UV-PDMS, 90UV-MOPDMS and 135UV-MOPDMS was 8:14:21:12. The highest peak intensity of the -CH_3 umbrella mode appeared in 90UV-PDMS, which indicated this SLIS had the best infusion effect of MO. Hydrophilic groups inspired by UV irradiation are typically short-lived in air. However, it is reported that the hydrophilic groups are more stable in the presence of polar molecules, such as ethanol [34]. Therefore the ester groups in MO could stabilize the hydrophilicity of PDMS substrate, which could be also observed in FTIR spectra. By comparing the FTIR peaks attributed to ester groups in the non-UV treated PDMS with those in the 90UV-PDMS, it was obvious that mutually MO could be infused and stored more efficiently in the cross-linked structure in PDMS after UV treatment, which was similar to the results of Ref [35].

The wettability of the coatings was evaluated by measuring the CA and SA in Table 1. The CA were just slightly different as all liquids were water-based, which indicated that the SLIS were engaged with good hydrophilic properties. This could be illustrated that UV treatment increased the surface energy of coatings and minimized the PDMS/MO interfacial tension, thus improving the hydrophilicity of SLIS [37].

Table 1
Static CA and SA of various liquid pollutants on the anti-fouling surface of 90UV-MOPDMS. The average results were presented after the tests were carried out three times.

Liquid pollutants	CA/°	SA/°
Water	80.2 ± 1.0	9.2 ± 0.9
Cola	78.6 ± 1.0	10.2 ± 0.3
Soy sauce	77.5 ± 0.6	10.5 ± 0.1
Coffee	75.4 ± 0.8	11.4 ± 0.6
Milk	73.4 ± 0.3	14.3 ± 0.5

3.3. *Anti-fouling and self-cleaning performance*

To evaluate the anti-fouling and self-cleaning performance, we investigated the wettability and resistance of the coatings against algal (such as Chlorella), daily liquid pollutants (including dyed water, cola, soy sauce, milk and coffee) and other typical common dirt (water and oil based stamp, earth and Fe_2O_3 for example).

All droplets were slipped off the coatings easily on a tilted platform without leaving any trace to study the sliding behavior. Compared with some recently similar results like coatings fabricated by hydrolytic condensation of methyltrimethoxysilane, whose SA values were from 17° to 24° [38], the SA of water in our study was just 9.2° and other values were also quite low (from 10° to 14°). These showed our SLIS surfaces exhibited excellent liquid repellency, which is owing to the smooth surface with relatively low surface energy [39].

The SLIS coatings were proven with excellent anti-fouling properties for various fluids regardless of their composition, showing anti-fouling properties for daily used liquids such as cola, soy sauce, milk, coffee. In Table 1, the CA and SA (the maximum SA value is 14.3° and less than 15°) of all kinds of liquids on 90UV-MOPDMS were shown. Therefore, the samples were placed on a platform with an inclination of 15°, and 5 μL of liquid to be tested was dropped onto the surface using a micro-injector. The whole process was observed and recorded with a high-speed camera.

On the bare PDMS, these liquids stick to the surface, as shown in Fig. 4(a). Although the liquids were semi-spherical in shape rather than spreading on the surface, they still could not slide off the PDMS surface (shown in (b)). This meant that even the smooth PDMS surface showed relatively enhanced hydrophobicity (large CA), but no liquid repellency. On the contrary, SLIS (90UV-MOPDMS for example) showed good liquid repellency regardless of what kind of liquid pollutant in Fig. 4(c) to (g), where all the liquid pollutants rolled away rapidly. The liquid pollutants were accelerated by the component of gravity (g) along the sliding direction, so the average velocities of different liquid pollutants (v_p) on the SLIS surface were calculated in Table 2 to describe their sliding

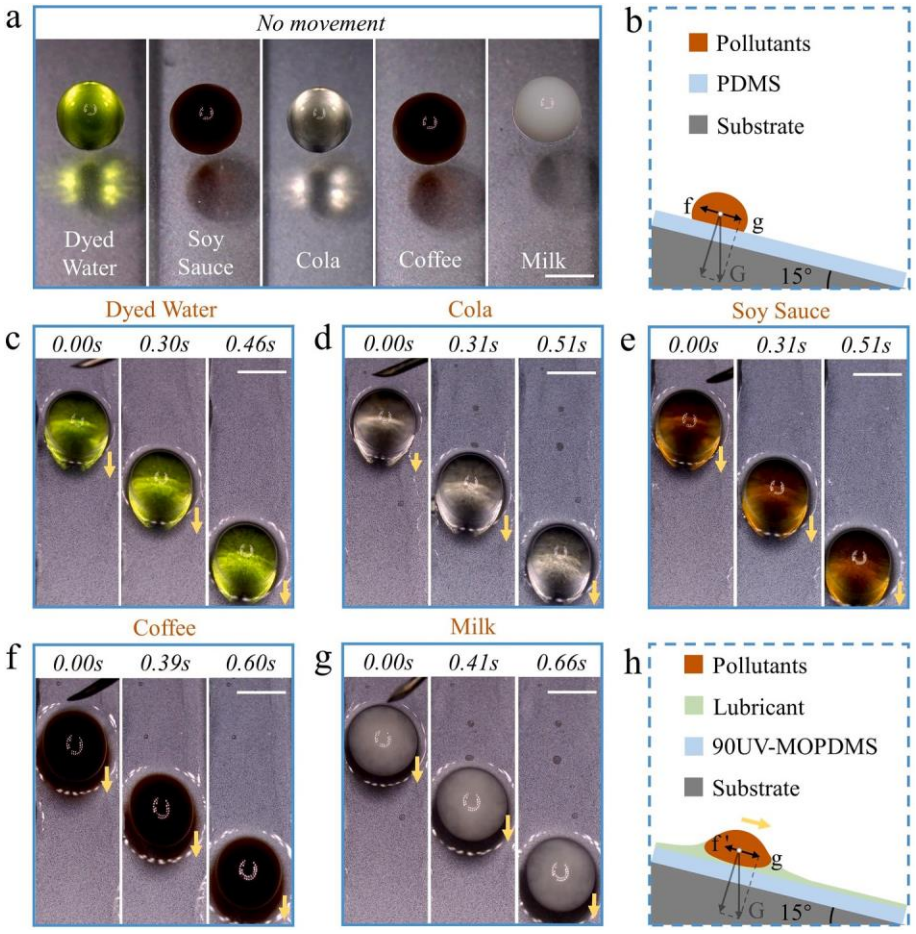

Fig. 4. Anti-fouling performance of the bare PDMS and SLIS: (a, b) kinds of daily used liquids on PDMS and the corresponding schematic diagram; (c-h) captures of all liquid pollutants rolling away and the corresponding schematic diagram. All scale bars are 2 mm.

Table 2
Average detachment velocity of different liquid pollutants on SLIS surface.

Liquid pollutants	Water	Cola	Soy sauce	Coffee	Milk
Average velocity/mm·s^{-1}	11.65	10.58	10.54	9.05	8.37

behaviors.

$$v_p = d/t_p$$

In the formula, v_p is the average velocities of liquid pollutant; d is the constant distance for the liquid pollutant sliding; and t_p is the time that pollutant took to slide the whole distance d.

It could be concluded that there was a very slight difference among them and all pollutants ran the 6 mm distance quite fast (within 0.7 s), even though the velocities of coffee and milk were a little lower because of holding more contamination. In Fig. 4(h), a schematic diagram was drawn to explain how the pollutants slide away. The secreting lubricant formed a uniform film on the surface and acted as the conveyor belt, where the liquid pollutant could be easily transported by gravity (G). Due to the liquid repellency of the MO lubricant itself, there is just a little adhesion (f′) between the liquid contaminant and the lubricant film. Once the surface is tilted, the force on the contaminant in the direction of the surface will not be unbalanced, where the component of gravity (g) along the surface is more dominant and can easily drag the liquid contamination away.

The SLIS coating also displayed anti-fouling properties with water-based and oil-based stamps. In Fig. 5(a1), PDMS was stamped with water-based ink and the pattern '交通大学' could be observed clearly. Then, the pattern was washed with water but the mark was still visible. The same pattern was printed on 90UV-MOPDMS whereas the words were very vague because of the ink shrinking behaviors (Fig. 5(a2)). After washing, the stamp was completely wiped. A similar phenomenon appeared on these two coatings when the oil-based stamp was used to test their anti-fouling ability. In conclusion, once stamped on the bare PDMS, the ink immediately spreads and sticks to the surface (Fig. 5(a1) and (b1)) even after being washed by pure water. Conversely, on the SLIS, the ink pattern shrank into tiny droplets and could be easily removed by the pure water (Fig. 5(a2) and (b2)). Whether the stamp had just been printed or been washed with water, the contrast between these two was quite obvious.

The anti-fouling performance could be proved with sand particles and daily common rust particles (Fe_2O_3) in Fig. 5(c) and (d). As shown in Fig. 5(c1) and (d1), the sand and Fe_2O_3 particles on bare PDMS were not efficiently removed by the water droplet. Water droplets of 1 mL were dropped onto the surface and then the samples were tilted vertically, but the particles left obvious traces. On the contrary, these two kinds of particles on the SLIS coating could be fully washed by water droplets and rolled down from the surface, owing to the lubricant film (Fig. 5(c2) and (d2)).

After the above experimental verification, SLIS has demonstrated excellent liquid repellency in the face of various common liquid pollutants in daily life. At the same time, on the surface of SLIS, solid contaminants can be also easily removed by water. The liquid repellency of SLIS is due to the lubricating layer, which repels liquids with a wide range of surface tensions [40].

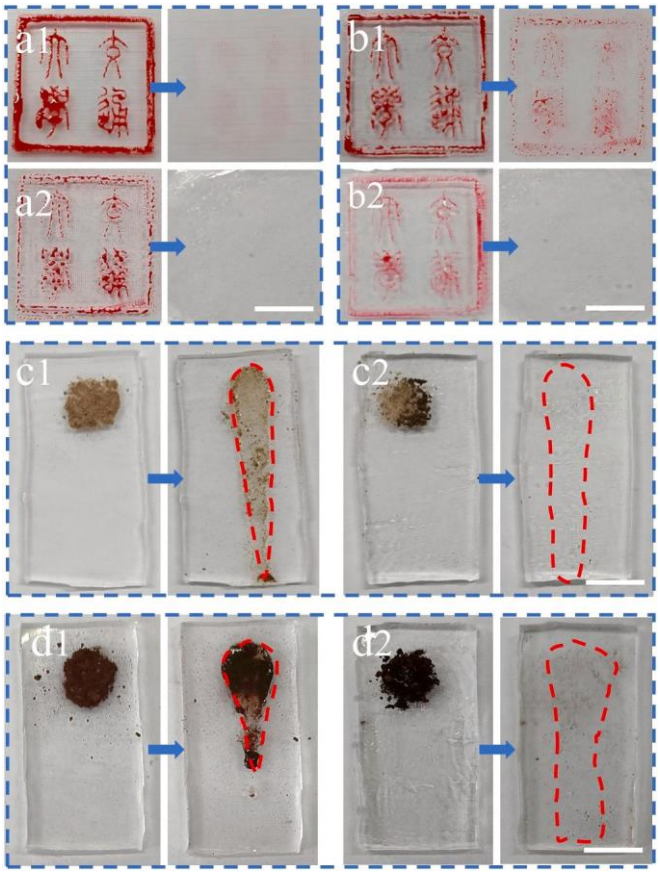

Fig. 5. Remove of water-based stamps on (a1) PDMS, (a2) SLIS; oil-based stamp on (b1) PDMS, (b2) SLIS; sand particles on (c1) PDMS, (c2) SLIS; and daily common rust particles (Fe_2O_3) on (d1) PDMS, (d2) SLIS; using 1 mL water droplets. All scale bars are 1 cm.

Fig. 6(g) demonstrated the anti-biofouling test process of coatings, which was totally under the same conditions as the Chlorella nutrition process. Fig. 6(a) to (f) were the morphological images of #1 in clean water and #1 to #5 in Chlorella solution. In comparison, Fig. 6(a) showed the PDMS coating immersed in pure water, and Fig. 6(b) dis- played how PDMS behaved in a solution rich with Chlorella: simple PDMS just could not withstand the fouling organisms inhibiting. On the contrary, the SLIS showed quite anti-biofouling ability in Fig. 6(c) to (f), among which the surface of #4 was very clean with the fewest inhibition of Chlorella. In order to better visualize the anti-biofouling ability of different coatings, surfaces were meshed and the colonized Chlorella per regions was counted. Results were shown in Fig. 6(h). It is quite obvious that there was an order of magnitude difference in the attachment density of Chlorella between SLIS and PDMS, revealing that SLIS exhibited excellent anti-biofouling performance and 90UV-MOPDMS behaved the best. It is well known that surface morphology, surface tension and chemical composition all have critical effects on the adhe- sion behaviors of microorganisms. The stable and uniform MO lubricant film can directly protect the surface from microorganisms and then significantly disrupt biological adhesion [41], which explains the outstanding anti-fouling and self-cleaning performance of 90UV-MOPDMS.

3.4. Evaluation of anti-corrosion performance

The anti-corrosion performance is a significant property of surfaces for preparing the surfaces applied in a harsh and complicated marine environment. To evaluate the corrosion resistance performance of the samples, electrochemical corrosion tests were conducted in 3.5 % NaCl solution to simulate the potentiodynamic polarization [42]. The Tafel curve is a portion of the polarization curve in the strongly polarized region. All Tafel polarization curves of various coatings are depicted in Fig. 7(a) and the parameters obtained from Tafel curves such as corrosion potential (E_{corr}) and corrosion current density (i_{corr}) are summa- rized in Fig. 7(b). According to relational literature, the higher the Ecorr, the better the corrosion resistance. The lower the icorr, the slower the corrosion velocity [43,44]. It could be seen from the graph that for all coatings, the Ecorr gradually increased at first, while the 135UV-MOPDMS coating declined, so the #5 showed the highest corrosion potential of −0.216 V. While the icorr presented the converse tendency: increasing first until #5 and then decreasing. The graph showed that #5 exhibited the lowest corrosion current density of 1.6×10^{-6} A, which reduced one o4rder of magnitude compared to #1 (6.1×10^{-5} A). By contrast, it could be concluded that the 90UV-MOPDMS coating showed the best corrosion resistance ability.

EIS measurements were employed to further investigate the anti-corrosion characteristics of the samples. Fig. 8(a) to (c) displayed the corresponding Bode modulus, Bode plots of phase angle and Nyquist plots Electrochemical Impedance Spectroscopy, respectively. Typically, the impedance values at a low measured frequency of 0.01 Hz ($|Z|_{0.01\ Hz}$) could better reflect the barrier properties of a coating system. The higher $|Z|_{0.01\ Hz}$ values mean more excellent barrier properties. From #1 to #5, the $|Z|_{0.01\ Hz}$ was sharply increased from $10^6\ \Omega\ cm^2$ to $10^{11}\ \Omega\ cm^2$, and then declined to $10^8\ \Omega\ cm^2$ of #6. Apparently, the corrosive process occurred at the metal/solution interface for #1 (bare Q235) while others showed attractive corrosion protection performance, whereas the #5 (90UV-MOPDMS) investigated the best anti-corrosion property. In Fig. 8 (b), the phase angle plots of #5 showed only one peak which corresponded to one time constant, indicating that the corrosive mediums did not arrive at the metal interface and the coating still acted as a good barrier. Except #5, the second peak appeared in other plots at the low frequency region, which illustrated that the second time constant showed up and those coatings all showed different degrees of corrosion. It is well-known that in Nyquist plots, the larger axial radius of a semi-elliptical arc indicated the better corrosion resistance of the coating. Therefore, it was evident that 90UV-MOPDMS displayed the best anti-corrosion performance from Fig. 8(c). It could be also observed that the capacitance of the 90UV-MOPDMS was rather larger than other surfaces. Generally, R_c is used to represent the degradation and porosity of the coating, whose value would decrease while the prolongation of time because of the continuous penetration of corrosive media. In Fig. 8 (d), #5 showed the highest value of R_c. Therefore, considering these evaluation criteria based on various aspects, the 90UV-MOPDMS exhibited the best corrosion resistance property, owing to the densest MO lubricating layer inside the coating, which was observed in the FTIR spectra.

The impedance data were analyzed by equivalent circuit models in Fig. 9. Generally, the electrical equivalent circuit for R (QR) (Fig. 9b) was employed to fit the EIS data at the initial stage of immersion. In this stage, the corrosive medium had not reached the coating/metal interface and no corrosion of metal substrate occurred, expressing as one time constant in the phase angle Bode plots. With the extension of immersion time, the corrosion medium gradually diffused to the coating/metal interface and induced metal corrosion. The second time constant was generated at the low frequency of the phase angle plots, and the impedance data were fitted by the electrical equivalent circuit of R(Q(R (QR))) (Fig. 9c) [45].

To explain the totally different anti-corrosion behaviors of samples, three corrosion resistance mechanism diagrams were displayed in Fig. 10. Fig. 10(a) depicted the invalid anti-corrosion coating, which corresponded to the pure PDMS coating in NaCl solution. In this case, the sodium ions, water molecules and dissolved oxygen in the solution could easily pass through the coating and carry out electrochemical corrosion on the surface of the substrate. In Fig. 10(b), both the densities of infusion lubricant and the SiO_x layer are related to the ability to resist

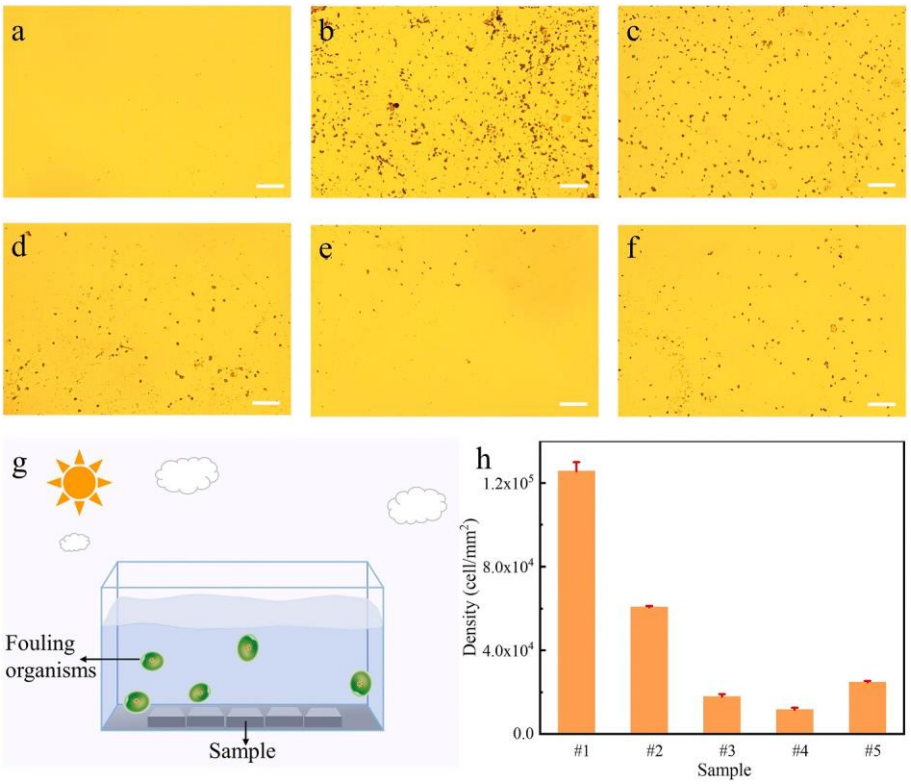

Fig. 6. The test about inhibition of Chlorella attachment (#1 to #5 are: Bare PDMS, 0UV-MOPDMS, 45UV-MOPDMS, 90UV-MOPDMS and 135UV-MOPDMS). All scale bars are 10 μm.

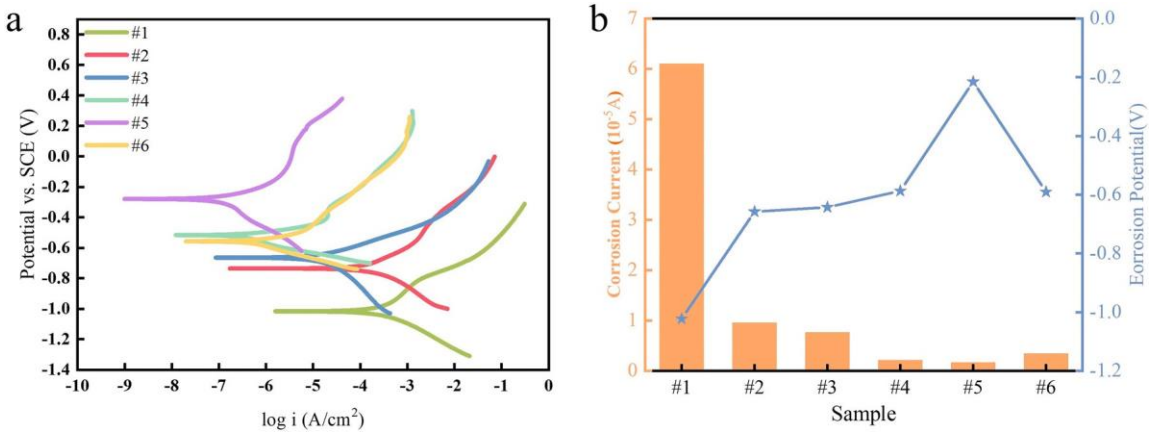

Fig. 7. (a) The Tafel curves of all samples in 3.5 wt% NaCl solution; (b) electrochemical polarization measurement electrochemical parameters (#1-Bare Substrate; #2-PDMS; #3-0UV-MOPDMS; #4-45UV-MOPDMS; #5-90UV-MOPDMS; #6-135UV-MOPDMS).

the sodium ion and dissolved Oxygen. When MO was increasing and SiO_x layer is getting denser like 90UV-MOPDMS, the coating exhibited a more effective protective function, which was shown in Fig. 10(c). The mechanism could be vividly explained by FTIR spectra. According to the FTIR spectra, the characteristic absorption peak at 1095 cm^{-1}, which was owing to Si–O–Si bond anti-symmetric stretching vibration, was compared to describe the cross-linking situation of PDMS after the UV irradiation. The lubricant infusion amount was same as the intensity of Si–O–Si bond, which was attributed to the formation of the oxidized surface layer of SiO_x [46]. However, long UV treatments would cause partial surface degradation and volume reduction [47]. By analyzing the FTIR spectra, we concluded that under the UV treatment conditions defined in this study, the SiO_x layer of 90UV-MOPDMS possessed the highest density in the samples with different irradiation durations.

3.5. Mechanical, thermal and chemical durability

Through the experiments in the previous sections, we have demonstrated that the SLIS coatings (especially 90UV-MOPDMS) showed excellent antifouling, self-cleaning, anti-corrosion and drag reduction properties. However, practical applications of anti-fouling coatings are always facing the handicap of durable mechanical, thermal and chemical stability. Therefore, the comprehensive durability of the coatings was carried out by various tests.

According to the mechanism analysis before, the maintenance of MO in the coatings played a considerable role in antifouling, anti-corrosion and drag reduction performances. Thus, the fluorescence signal was detected on different samples at the beginning and one week later, and fluorescent intensity was calculated with a semi-quantitative method

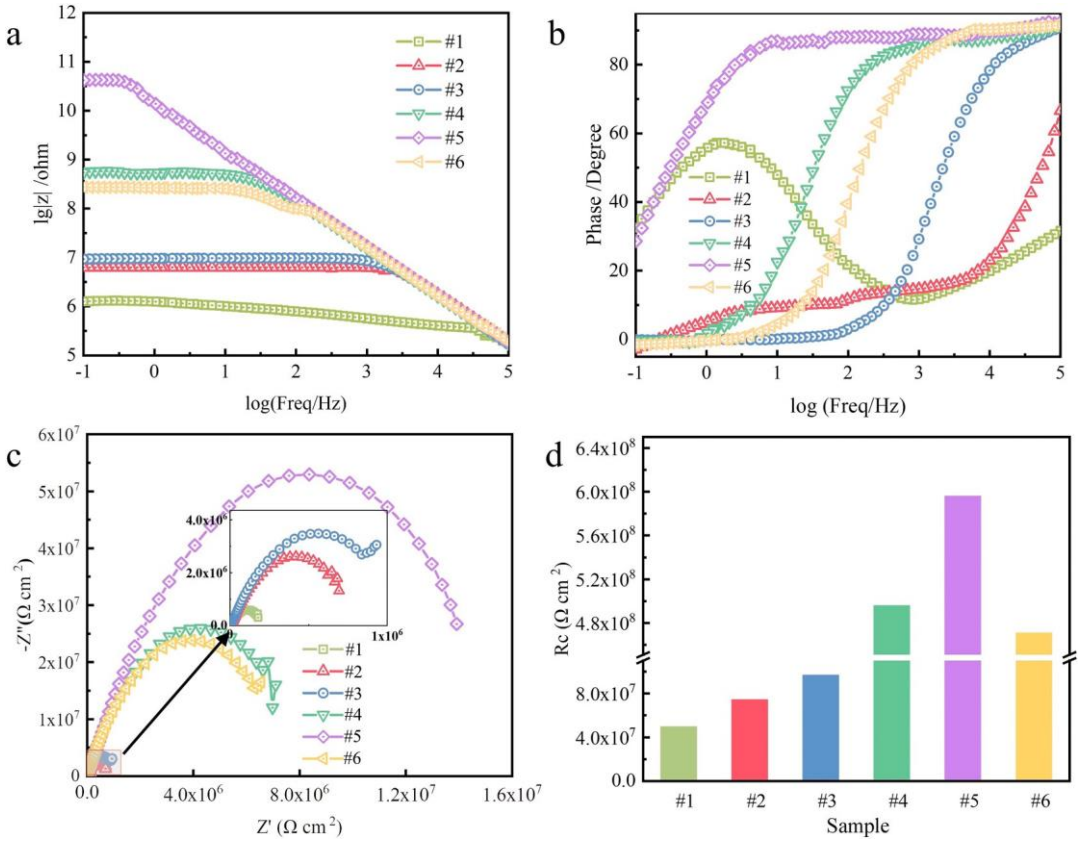

Fig. 8. The (a) Bode modulus plots, (b) bode phase angle plots and (c) Nyquist plots in Electrochemical Impedance Spectroscopy; (d) coating resistance of samples (#1-Bare Substrate; #2-PDMS; #3-0UV-MOPDMS; #4-45UV-MOPDMS; #5-90UV-MOPDMS; #6-135UV-MOPDMS).

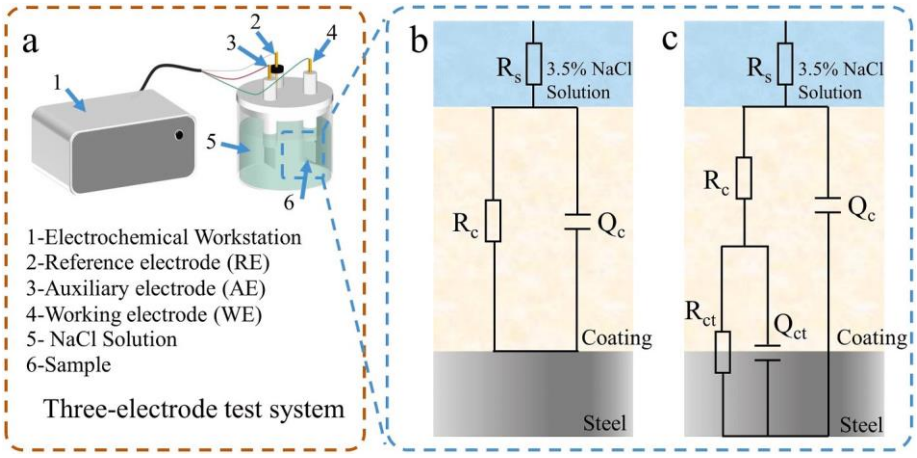

Fig. 9. The equivalent electric circuit models [(b): R (QR), (c): R (Q (R (QR)))] were employed to simulate the impedance data. Where R_s corresponds to solution resistance, R_c and R_{ct} represent the coating resistance and charge transfer resistance, Q_c stands for the constant phase element of coating capacitance, Q_{ct} is the constant phase element of double layer capacitance.

[48]. The samples were shone with a focused beam of monochromatic laser light of wavelength k ~~5~~61 nm and the fluorescence signals were captured through the pinhole of a confocal microscope. The lubricant MO was dyed with the fluorescent dye Oil Red O (emission wavelengths kem from 565 to 650 nm), which allowed us to visualize the spatial infusing situation of the MO in PDMS. During that week, all the samples were put in a flowing water environment to imitate the actual working conditions. Original and changed fluorescent intensities were displayed in Fig. 11(a). For the original samples, 90UV-MOPDMS showed the highest intensity which was about 8.44 times of pure PDMS, while the intensities of 45UV-MOPDMS and 135UV-MOPDMS were just 2.87 and 3.38 times of that of PDMS. One week later, 90UV-MOPDMS showed the smallest attenuation amplitude in fluorescence intensity, which was just 12.5 %. However, the attenuation for 135UV-MOPDMS, 45UV-MOPDMS and PDMS were 66 %, 80 % and 82.5 %, respectively. In Fig. 11(b), CA and particularly SA were measured on the SLIS samples after the scour of flowing water. For the original samples, 90UV- MOPDMS showed the smallest SA which was about 9.2°, while the SAs of 0UV-MOPDMS, 45UV-MOPDMS and 135UV-MOPDMS were 32.5°, 10.4° and 12.1°, respectively. Among all SLIS, 90UV-MOPDMS

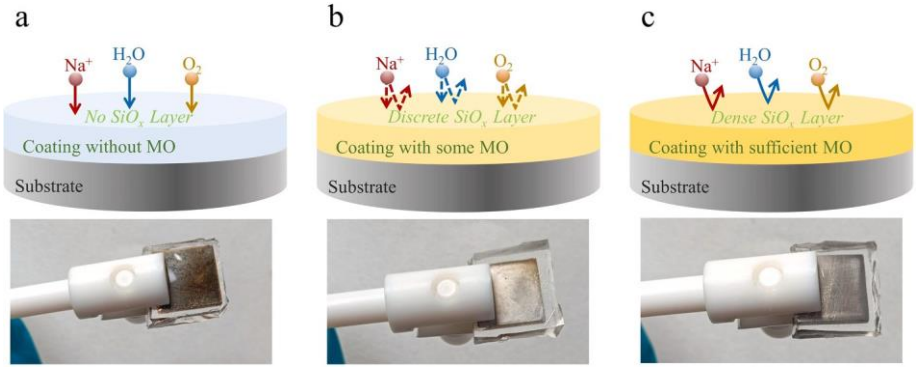

Fig. 10. Three anti-corrosion mechanism diagrams and actual corresponding substrate corrosion under protection of different coatings: the (a) invalid, (b) feasible and (c) efficient anti-corrosion coatings.

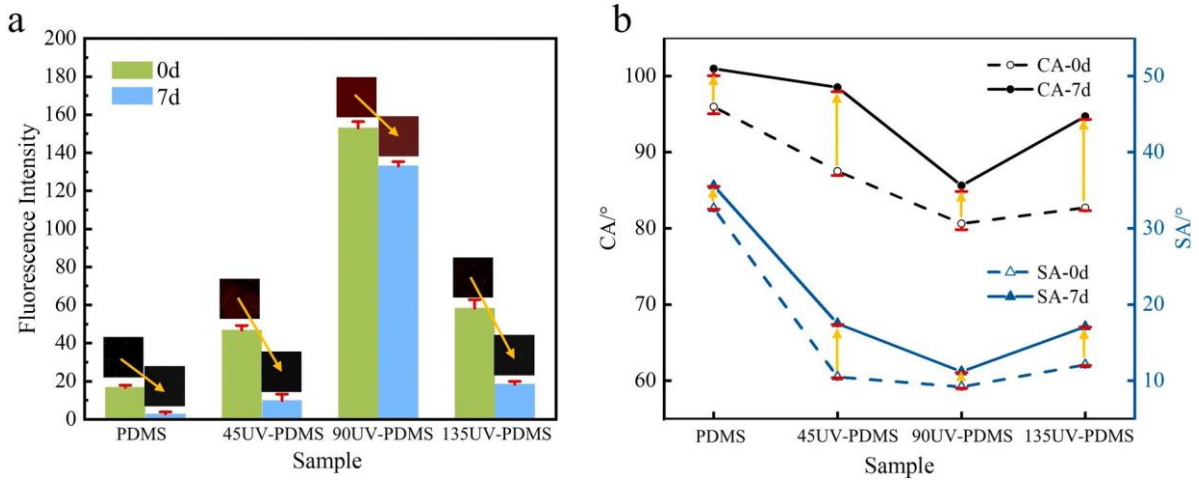

Fig. 11. Characterization of durable and long-term lubricant release behavior: (a) Fluorescence intensity change and (b) wettability change in flowing water environment for one week.

really displayed the outstanding water repellency. After souring for 7 days, SA of 90UV-MOPDMS increased but still showed the smallest value at 11.2° while the SAs of 0UV-MOPDMS, 45UV-MOPDMS and 135UV-MOPDMS increased to 35.6°,17.5° and 17.1°, respectively. The CAs also displayed similar trend, revealing the lubricant was slowly released. Results indicated that SLIS showed superior durability from the perspective of liquid repellency. And 90UV-MOPDMS displayed the best performance and exhibited the highest efficiency in both the lubricant infusion and long-term lubricant release, which may be an optimized condition for designing the long-term stable service SLIS specimen.

The durability of anti-corrosion is also a vital index for evaluating the applications of coatings [42]. Three UV treatment experimental specimens were chosen to observe the durable electrochemical anti-corrosion performance. After being immersed in a flowing water environment for seven days, the samples were tested in 3.5 wt% NaCl solution circumstance and corresponding Tafel plots were obtained in Fig. 12(a). Obviously, the E_{corr} of 90UV-MOPDMS was still the highest. The calculated parameters were displayed in Fig. 12(b). It could be seen from the graph that even after timeless work, the E_{corr} and i_{corr} presented a very slight change. For E_{corr}, #5 decreased from —0.216 V to —0.307 V, and #4 and #6 also reduced a little. For i_{corr}, all coatings slightly rose and #5 increased from 1.6×10^{-6} A to 1.8×10^{-6} A. By contrast, it

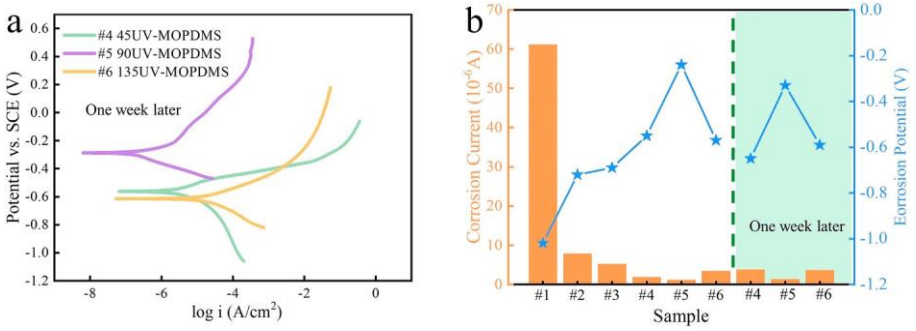

Fig. 12. Anti-corrosion persistence of SLIS deposed in flowing water environment for one week: (a) the Tafel curves of all samples in 3.5 wt% NaCl solution; (b) electrochemical polarization measurement electrochemical parameters.

could be concluded that the UV treated specimen investigated very strong durability and stability in anti-corrosion, and the 90UV-MOPDMS coating still showed the best corrosion resistance ability.

The mechanical stability of the coating can be proven by the cyclic stretch tests. The wettability and anti-fouling behavior of the 90UV-MOPDMS coating were tested after repeated pulls.

The surface wettability was measured after 250, 500, 750 and 1000 cycles, respectively, and the variation laws of contact angle (CA) and sliding angle (SA) were obtained as shown in Fig. 13(a). In order to ensure the accuracy of the measurement results, pure water was added dropwise to different areas of the sample in each group of experiments and the measurement was repeated at least 3 times. The CA and the SA both increased gradually with the increase of stretch cycles. The range of CA was stably kept around 93°, which meant the coating was partly dried because of the secretion of MO while the surface energy was just slightly decreased by cyclic pull. In addition, the SA still remained very low (under 11°), meaning the liquid pollutants could roll away easily. As shown in Fig. 13(b), a self-cleaning performance test was conducted on pure PDMS and SLIS after 1000 times stretch. The samples were immersed in concentrated coffee and then removed. The coffee could still gather and slide away from the SLIS coating without leaving any marks, but attached and polluted the PDMS coating, which vividly demonstrated the SLIS coating has good mechanical stability even after long-term pulls.

Referring to previous studies [49,50], the coating would be undermined by soaking in saline solutions and hot water, thus reducing the anti-fouling performance. As shown in Fig. 14, both MOPDMS and 90UV-MOPDMS were placed in a continuously heated 60 °C high-temperature water bath environment and a high-saline solution with a mass fraction of 3.5 % NaCl for a week. During immersion, the lubricant MO was lost due to the saline and high temperature environment. Therefore, the weight of the samples was recorded to describe the loss of lubricant contained in samples every 24 h. Fig. 14(a) and (b) showed the loss of lubricant for MOPDMS and 90UV-MOPDMS immersed in hot water for a week. As shown in Fig. 14(a), the weight of 90UV-PDMS was significantly increased after MO infusion, which indicated that more lubricants were infused. When the hot water was used to wash the surface, both of 90UV-PDMS and MOPDMS experienced a process of weight reduction. The reflected the releasing rate of the MO was defined as the following formula:

$$Rn = (m_0 - m_n)/m \times 100\%$$

In the formula, m is the weight of the coating before MO infusion; m_0 is the initial weight after MO infusion; and m_n is the weight of the sample after n days' releasing.

In Fig. 14(a), the orange area meant the lubricant infusion stage, and it could be clearly noticed that 90UV-PDMS could significantly absorb MO compared to PDMS; the blue area was the lubricant release stage. Even experiencing one week of washing in a high-temperature water environment, 90UV-MOPDMS still showed good long-time resistance to liquid pollutants (dyed water here in the graph). Fig. 14(b) displayed the difference in lubricant loss rate between these two coatings. It was very obvious that the lubricant loss of 90UV-MOPDMS in hot water was much slower than that of MOPDMS, emphasizing the former better thermal stability. In saline solutions, coatings exhibited similar processes to those in hot water, which was demonstrated in Fig. 14(c). In addition, Long-time resistance to liquid pollutants (milk here in the graph) was also recorded. However, the releasing weight ratio (R_n) revealed the discrepancy under two different circumstances: although the coatings still behaved well on the durable anti-fouling aspect in saline solution, the velocities of MO loss were nearly close. The mechanical, thermal and chemical durability of SLIS is due to the self-healing performance of the lubricant layer. Damaged lubricant film parts can be mended by oil flow from the infusion lubricating layer [51] and the previous characterization of the efficient infusion of lubricant guarantees this self-healing performance.

4. Conclusions

In the work, a facile and novel method of fabricating SLIS with stable anti-fouling and anti-corrosion performance was proposed. Five different coatings (MOPDMS, 45UV-MOPDMS, 90UV-MOPDMS and 145UV-MOPDMS) were prepared based on UV irradiation time. Release, tribological and mechanical tests were used to carefully analyze the performance of the coatings. The experimental results were as follows:

- An efficient lubricant infusion method was used to construct SLIS by altering the PDMS cross-linking process with direct UV irradiation. The prepared coating has good transparency and smoothness.
- Compared to the reference substrate, SLIS treated with 90 min UV irradiation (90UV-MOPDMS) showed the greatest anti-fouling and anti-corrosion performance, which was demonstrated by the functionality of durable lubricating MO coating covering on the PDMS and the cross-linked dense SiO_x layer owing to UV irradiation. The presence of the lubricant effectively reduced the adhesion of contaminants and isolated the exchange of ions and water between the solution and the protected substrate.
- Release experiment revealed that the SLIS possessed durable mechanical, chemical and thermal stabilities. It was demonstrated that because of the synergistic effect of inhibitor MO and the dense SiO_x layer, the antifouling layer can be used for a long time, thereby endowing coating with remarkable stability.

We foresee that the SLIS coatings have broad applications in marine

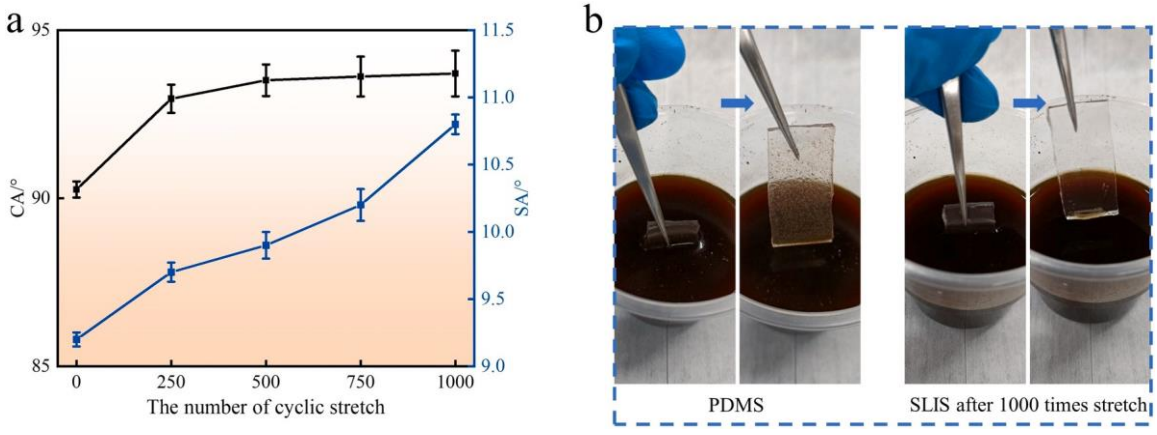

Fig. 13. (a) Variation of CA under cyclic stretching and (b) the remove of coffee on SLIS after repeated stretch.

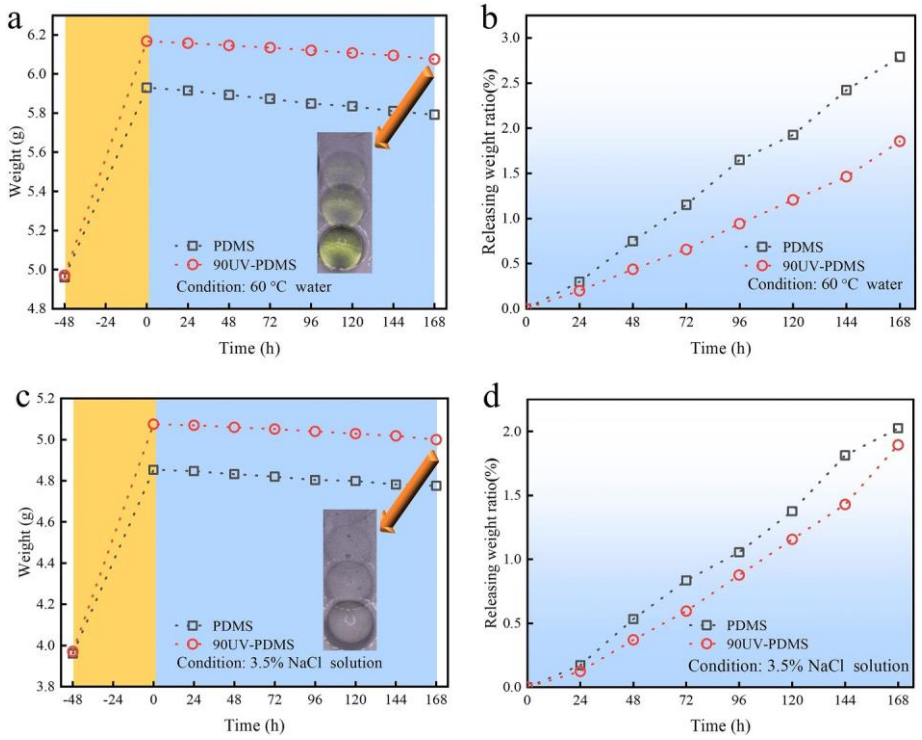

Fig. 14. Weight change and releasing weight ratio of MOPDMS and 90UV-MOPDMS under: (a, b) high temperature and (c, d) high salt environment for one week, respectively.

equipment. The coatings may significantly save energy, cost, and labor in cleaning and maintaining underwater surfaces.

CRediT authorship contribution statement

Hao Yang: Writing – original draft, Project administration, Methodology.
Liguo Qin: Writing – review & editing, Supervision.
Fei Wang: Investigation, Data analysis.
Fagla Jules Mawignon: Investigation.
Mochen Dong: Investigation.
Yuhao Wu: Investigation.
Yali Zhang: Investigation, Data analysis.
Zeyu Ma: Investigation.

Declaration of competing interest

The authors have no competing interests to declare that are relevant to the content of this article.

Data availability

Data will be made available on request.

Acknowledgements

The authors acknowledge the National Natural Science Foundation of China (51975458 and 51605370), the financial support from the China Scholarship Council, China Postdoctoral Science Foundation funded project (2020M673377 and 2020T130510), Key Research and Development Program of Shaanxi Province (2022SF-069) and the Natural Science Foundation of Shaanxi Province (2020JM-010).

References

[1] S.A. Gokulakrishnan, G. Arthanareeswaran, Z. Laszlo, G. Vereb, S. Kertesz, J. Kweon, Recent development of photocatalytic nanomaterials in mixed matrix membrane for emerging pollutants and fouling control, membrane cleaning process, Chemosphere 281 (2021), 130891.
[2] X. Han, J. Wu, X. Zhang, J. Shi, J. Wei, Y. Yang, B. Wu, Y. Feng, The progress on antifouling organic coating: from biocide to biomimetic surface, J. Mater. Sci. Technol. 61 (2021) 46–62.
[3] W. Yao, L. Wu, L. Sun, B. Jiang, F. Pan, Recent developments in slippery liquid-infused porous surface, Prog. Org. Coat. 166 (2022), 127836.
[4] X. Wu, M. Lui, X. Zhong, G. Liu, I. Wyman, Z. Wang, Y. Wu, H. Yang, J. Wang, Smooth water-based antismudge coatings for various substrates, ACS Sustain. Chem. Eng. 5 (3) (2017) 2605–2613.
[5] A.H. Nikoo, M.R. Malayeri, Incorporation of surface energy properties into general crystallization fouling model for heat transfer surfaces, Chem. Eng. Sci. 215 (2020), 115461.
[6] Z. Wang, Z. Zhou, W. Xu, D. Yang, Y. Xu, L. Yang, J. Ren, Y. Li, Y. Huang, Research status and development trends in the field of marine environment corrosion: a new perspective, Environ. Sci. Pollut. Res. 28 (39) (2021) 54403–54428.
[7] W. Dong, B. Li, J. Wei, N. Tian, W. Liang, J. Zhang, Environmentally friendly, durable and transparent anti-fouling coatings applicable onto various substrates, J. Colloid Interface Sci. 591 (2021) 429–439.
[8] Y.B. Li, T. Hu, B.C. Li, J.F. Wei, J.P. Zhang, Totally waterborne and highly durable superamphiphobic coatings for anti-icing and anticorrosion, Adv. Mater. Interfaces 6 (23) (2019).
[9] S. Amini, S. Kolle, L. Petrone, O. Ahanotu, S. Sunny, C.N. Sutanto, S. Hoon, L. Cohen, J.C. Weaver, J. Aizenberg, N. Vogel, A. Miserez, Preventing mussel adhesion using lubricant-infused materials, Science 357 (Aug. 18 TN.6352) (2017) 668–673.
[10] X. Lin, F. Lu, Y.N. Chen, N. Liu, Y.Z. Cao, L.X. Xu, Y. Wei, L. Feng, One-step breaking and separating emulsion by tungsten oxide coated mesh, ACS Appl. Mater. Interfaces 7 (15) (2015) 8108–8113.
[11] F. Li, R. Gao, T. Wu, Y. Li, Role of layered materials in emulsified oil/water separation and anti-fouling performance of modified cellulose acetate membranes with hierarchical structure, J. Membr. Sci. 543 (2017) 163–171.
[12] L.F. Zhang, G.J. He, D.F. Ye, N.N. Zhan, Y.S. Guo, W.J. Fang, Methacrylated hyperbranched polyglycerol as a high-efficiency demulsifier for oil-in-water emulsions, Energy Fuel 30 (11) (2016) 9939–9946.
[13] I. Karapanagiotis, P.N. Manoudis, Superhydrophobic and superamphiphobic materials for the conservation of natural stone: an overview, Constr. Build. Mater. 320 (2022), 115461.
[14] L. Qin, H. Yang, F.J. Mawignon, Y. Zhang, G. Dong, A facile method for fabricating super-slippery surface with long term and high-efficiency sustained release performance, Prog. Org. Coat. 174 (2023), 107275.

[15] B. Su, Y. Tian, L. Jiang, Bioinspired interfaces with superwettability: from materials to chemistry, J. Am. Chem. Soc. 138 (6) (2016) 1727–1748.
[16] A.B. Tesler, P. Kim, S. Kolle, C. Howell, O. Ahanotu, J. Aizenberg, Extremely durable biofouling-resistant metallic surfaces based on electrodeposited nanoporous tungstite films on steel, Nat. Commun. 6 (2015) 8649.
[17] J. Zhang, J. Zhao, W. Qu, X. Li, Z. Wang, One-step, low-cost, mussel-inspired green method to prepare superhydrophobic nanostructured surfaces having durability, efficiency, and wide applicability, J. Colloid Interface Sci. 580 (2020) 211–222.
[18] X. Lin, F. Lu, Y. Chen, N. Liu, Y. Cao, L. Xu, Y. Wei, L. Feng, One-step breaking and separating emulsion by tungsten oxide coated mesh, ACS Appl. Mater. Interfaces 7 (15) (2015) 8108–8113.
[19] L.L. Xiao, J.S. Li, S. Mieszkin, A. Di Fino, A.S. Clare, M.E. Callow, J.A. Callow, M. Grunze, A. Rosenhahn, P.A. Levkin, Slippery liquid-infused porous surfaces showing marine antibiofouling properties, ACS Appl. Mater. Interfaces 5 (20) (2013) 10074–10080.
[20] D.F. Cheng, C. Urata, M. Yagihashi, A. Hozumi, A statically oleophilic but dynamically oleophobic smooth nonperfluorinated surface, Angew. Chem. Int. Ed. 51 (12) (2012) 2956–2959.
[21] B. Li, B. Yu, Q. Ye, F. Zhou, Tapping the potential of polymer brushes through synthesis, Acc. Chem. Res. 48 (2) (2015) 229–237.
[22] T.-S. Wong, S.H. Kang, S.K.Y. Tang, E.J. Smythe, B.D. Hatton, A. Grinthal, J. Aizenberg, Bioinspired self-repairing slippery surfaces withpressure-stable omniphobicity, Nature 477 (Sep. 22 TN.7365) (2011) 443–447.
[23] S. Amini, S. Kolle, L. Petrone, O. Ahanotu, S. Sunny, C.N. Sutanto, S. Hoon, L. Cohen, J.C. Weaver, J. Aizenberg, Preventing mussel adhesion using lubricant-infused materials, Science 357 (6352) (2017) 668.
[24] Y. Lu, G. He, C.J. Carmalt, I.P. Parkin, Synthesis and characterization of omniphobic surfaces with thermal, mechanical and chemical stability, RSC Adv. 6 (108) (2016) 106491–106499.
[25] L.G. Qin, Z.Y. Ma, H.J. Sun, S. Lu, Q.F. Zeng, Y.L. Zhang, G.N. Dong, Drag reduction and antifouling properties of non-smooth surfaces modified with ZIF-67, Surf. Coat. Technol. 427 (127836) (2021).
[26] C. Wei, G. Zhang, Q. Zhang, X. Zhan, F. Chen, Silicone oil-infused slippery surfaces based on sol-gel process-induced nanocomposite coatings: a facile approach to highly stable bioinspired surface for biofouling resistance, ACS Appl. Mater. Interfaces 8 (50) (2016) 34810–34819.
[27] K. Doll, E. Fadeeva, J. Schaeske, T. Ehmke, A. Winkel, A. Heisterkamp, B. N. Chichkov, M. Stiesch, N.S. Stumpp, Development of laser-structured liquid-infused titanium with strong biofilm-repellent properties, ACS Appl. Mater. Interfaces 9 (11) (2017) 9359–9368.
[28] P. Wang, D. Zhang, S. Sun, T. Li, Y. Sun, Fabrication of slippery lubricant-infused porous surface with high underwater transparency for the control of marine biofouling, ACS Appl. Mater. Interfaces 9 (1) (2017) 972–982.
[29] S. Basu, H. Bui My, J.Q.I. Chua, D. Daniel, M.H. Ismail, M. Marchioro, S. Amini, S. A. Rice, A. Miserez, Green biolubricant infused slippery surfaces to combat marine biofouling, J. Colloid Interface Sci. 568 (2020) 185–197.
[30] S. Sunny, N. Vogel, C. Howell, T.L. Vu, J. Aizenberg, Lubricant-infused nanoparticulate coatings assembled by layer-by-layer deposition, Adv. Funct. Mater. 24 (42) (2014) 6658–6667.
[31] C. Zheng, G. Liu, H. Hu, UV-curable antismudge coatings, ACS Appl. Mater. Interfaces 9 (30) (2017) 25623–25630.
[32] R. Macedo, N.D. Marques, J. Tonholo, R.D. Balaban, Water-soluble carboxymethylchitosan used as corrosion inhibitor for carbon steel in saline medium, Carbohydr. Polym. 205 (2019) 371–376.
[33] Y. Feng, Y.F. Cheng, An intelligent coating doped with inhibitor-encapsulated nanocontainers for corrosion protection of pipeline steel, Chem. Eng. J. 315 (2017) 537–551.
[34] B. Kim, E.T.K. Peterson, I. Papautsky, Long-term stability of plasma oxidized PDMS surfaces, P. Ann. Int. IEEE Embs 26 (2004) 5013–5016.
[35] H.F. Lu, W.P. Yan, Z.H. Liu, J.C. Li, Hydrophilic surface modification of polydimethylsiloxane with UV/Ozone treatment, Spectrosc. Spectr. Anal. 36 (4) (2016) 1033–1037.
[36] P. Kowalik, D. Elbaum, J. Mikulski, K. Fronc, I. Kaminska, P.C. Morais, P.E. de Souza, R.B. Nunes, F.H. Veiga-Souza, G. Gruzel, R. Minikayev, T. Wojciechowski, E. Mosiniewicz-Szablewska, M. Szewczyk, M. Pawlyta, A. Sienkiewicz, M. Lapinski, K. Zajdel, P. Stepien, J. Szczepkowski, W. Jastrzebski, M. Frontczak-Baniewicz, W. Paszkowicz, B. Sikora, Upconversion fluorescence imaging of HeLa cells using ROS generating SiO2-coated lanthanide-doped NaYF4 nanoconstructs, RSC Adv. 7 (48) (2017) 30262–30273.
[37] S. Basu, B.M. Hanh, J.Q.I. Chua, D. Daniel, M.H. Ismail, M. Marchioro, S. Amini, S. A. Rice, A. Miserez, Green biolubricant infused slippery surfaces to combat marine biofouling, J. Colloid Interface Sci. 568 (2020) 185–197.
[38] W.R. Dong, B.C. Li, J.F. Wei, N. Tian, W.D. Liang, J.P. Zhang, Environmentally friendly, durable and transparent anti-fouling coatings applicable onto various substrates, J. Colloid Interface Sci. 591 (2021) 429–439.
[39] B. Masheder, C. Urata, A. Hozumi, Transparent and hard zirconia-based hybrid coatings with excellent dynamic/thermoresponsive oleophobicity, thermal durability, and hydrolytic stability, ACS Appl. Mater. Interfaces 5 (16) (2013) 7899–7905.
[40] Z.C. Yang, X.Y. He, J.F. Chang, C.Q. Yuan, X.Q. Bai, Facile fabrication of fluorine-free slippery lubricant-infused cerium stearate surfaces for marine antifouling and anticorrosion application, Surf. Coat. Technol. 415 (2021), 127136.
[41] J.L. Yin, M.L. Mei, Q.L. Li, R. Xia, Z.H. Zhang, C.H. Chu, Self-cleaning and antibiofouling enamel surface by slippery liquid-infused technique, Sci. Rep.-Uk 6 (25924) (2016).
[42] V.I. Naumov, A.A. Kalinina, V.V. Isaev, A.V. Borisov, Anodic dissolution of iron in the solutions simulating the composition of corrosive exometabolites of organotrophic bacteria, Prot. Met. Phys. Chem. Surf. 57 (7) (2021) 1380–1387.
[43] E.H. Ramirez-Soria, U. Leon-Silva, T.E. Lara-Ceniceros, L. Bazan-Diaz, R. C. Advincula, J. Bonilla-Cruz, Graphene oxide bifunctionalized with NH2/NH3 + and their outstanding-performance against corrosion, Appl. Surf. Sci. 561 (2021).
[44] N. Thongchuea, E. Warinsiriruk, N. Phuraya, P. Sa-Ngasoongsong, Corrosion behavior on cerclage-wire joining using laser welding, AIP Conf. Proc. 2279 (2020), 080002 (8 pp.)-080002 (8 pp.).
[45] C. Yang, W.J. Xu, X. Meng, X.L. Shi, L.H. Shao, X.L. Zeng, Z.F. Yang, S.J. Li, Y. T. Liu, X.N.A. Xia, A pH-responsive hydrophilic controlled release system based on ZIF-8 for self-healing anticorrosion application, Chem. Eng. J. 415 (2021), 128985.
[46] H.-F. Lu, W.-P. Yan, Z.-H. Liu, J.-C. Li, Hydrophilic surface modification of polydimethylsiloxane with UV/Ozone treatment, Spectrosc. Spectr. Anal. 36 (4) (2016) 1033–1037.
[47] A. del Campo, A. Nogales, T.A. Ezquerra, J. Rodriguez-Hernandez, Modification of poly(dimethylsiloxane) as a basis for surface wrinkle formation: chemical and mechanical characterization, Polymer 98 (2016) 327–335.
[48] D. Li, Z. Zhu, J. Li, L. Wang, Accuracy research of minerals with high loss of ignition during X-ray fluorescence spectrometry semi-quantitative analysis, Rock Miner. Anal. 39 (1) (2020) 135–142.
[49] D.F. Cheng, B. Masheder, C. Urata, A. Hozumi, Smooth perfluorinated surfaces with different chemical and physical natures: their unusual dynamic dewetting behavior toward polar and nonpolar liquids, Langmuir 29 (36) (2013) 11322–11329.
[50] B. Shang, M. Chen, L.M. Wu, Fabrication of UV-triggered liquid-repellent coatings with long-term self-repairing performance, ACS Appl. Mater. Interfaces 10 (37) (2018) 31777–31783.
[51] C. Liu, Y.L. Li, C.G. Lu, Y. Liu, S.L. Feng, Y.H. Liu, Robust slippery liquid-infused porous network surfaces for enhanced anti-icing/Deicing performance, ACS Appl. Mater. Interfaces 12 (22) (2020) 25471–25477.